Sains Malaysiana 55(4)(2026): 730-745
http://doi.org/10.17576/jsm-2026-5504-12

Fractional-Order Modeling of Dengue Virus Dynamics with Predator-Prey Interactions

(Pemodelan Tertib Pecahan Dinamik Virus Denggi dengan Interaksi Pemangsa-Mangsa)

SARINAH BANU MOHAMED SIDDIK[1], MATTHEW O. ADEWOLE[2,3,*], NEWTON I. OKPOSO[4], TAYE SAMUEL FANIRAN[5,6] & FARAH AINI ABDULLAH[3,7]

[1]*Department of Mathematical Sciences, Faculty of Intelligent Computing, Universiti Malaysia Perlis, Kampus Alam UniMAP, Pauh Putra, 02600 Arau, Perlis, Malaysia*
[2]*Mathematics Programme, Bowen University, Iwo, Nigeria*
[3]*School of Mathematical Sciences, Universiti Sains Malaysia 11800 USM Pulau Pinang, Malaysia*
[4]*Department of Mathematics, Delta State University, Abraka, PMB 1, Delta state, Nigeria*
[5]*F.I. Proctor Foundation, University of California, San Francisco, USA*
[6]*Lead City University, Ibadan, Nigeria*
[7]*Nonlinear Dynamics Research Center (NDRC), Ajman University, Ajman, UAE*

Received: 15 May 2025/Accepted: 7 April 2026

#Both S.B.M. Siddik and M.O. Adewole contributed equally and thus are joint first authors

ABSTRACT

This study analyzes a Caputo-Fabrizio fractional differential model to capture dengue transmission dynamics, incorporating predator-prey interactions. The analysis confirms the existence, uniqueness, and positivity of solutions, establishing the model as biologically meaningful and well-posed. The disease-free equilibrium is identified, and its asymptotic stability is evaluated under specific conditions. An implicit numerical scheme is proposed, and its performance is compared to the two-step Adams–Bashforth scheme, showing enhanced accuracy and stability. Parameter estimation through model fitting aligns the model with observed real-world data. Sensitivity analysis using Latin Hypercube Sampling-Partial Rank Correlation Coefficient (LHS-PRCC) shows key parameters influencing the dynamics of dengue transmission. The results show that while predator-prey interactions help mitigate dengue transmission, they are insufficient for complete disease eradication. This highlights the need for complementary control measures, such as vector control, public health education, and improved healthcare systems, to effectively reduce transmission.

Keywords: Numerical scheme; predator-prey; sensitivity analysis

ABSTRAK

Kajian ini menganalisis model pembezaan pecahan Caputo-Fabrizio untuk menunjukkan dinamik penularan denggi, menggabungkan interaksi pemangsa-mangsa. Analisis ini mengesahkan kewujudan, keunikan dan kepositifan penyelesaian, menjadikan model tersebut bermakna secara biologi dan tepat. Keseimbangan bebas penyakit dikenal pasti dan kestabilan asimptotiknya dinilai di bawah keadaan tertentu. Skema berangka tersirat dicadangkan dan prestasinya dibandingkan dengan skema Adams-Bashforth dua langkah, menunjukkan ketepatan dan kestabilan yang dipertingkatkan. Anggaran parameter melalui pemadanan model menyelaraskan model dengan data dunia sebenar yang diperhatikan. Analisis sensitiviti menggunakan Pekali Korelasi Peringkat Separa-Pensampelan Hiperkubus Latin (LHS-PRCC) mendedahkan parameter utama yang mempengaruhi dinamik penularan denggi. Keputusan menunjukkan bahawa walaupun interaksi pemangsa-mangsa membantu mengurangkan penularan denggi, ia tidak mencukupi untuk pembasmian penyakit sepenuhnya. Ini menonjolkan keperluan untuk langkah kawalan pelengkap, seperti kawalan vektor, pendidikan kesihatan awam dan sistem penjagaan kesihatan yang lebih baik untuk mengurangkan penularan secara berkesan.

Kata kunci: Analisis sensitiviti; pemangsa-mangsa; skema berangka

INTRODUCTION

Dengue is a significant viral public health threat in tropical and subtropical regions, transmitted primarily by female *Aedes aegypti* mosquitoes (Gutierrez-Barbosa et al. 2019; Srivastav & Ghosh 2019). The disease is caused by five distinct serotypes and can be fatal (Zhu, Lin & Zhang 2020).

Global incidence has increased 30-fold over 50 years, with 50 million annual infections (Guzman et al. 2010; WHO 2016). Lacking specific vaccines or medications, control relies on reducing transmission (Charette et al. 2017). Biological control strategies, utilizing natural predators like dytiscid beetles, fish, and amphibians, are employed to manage mosquito populations.

Mathematical modeling is vital for understanding dengue transmission, using diverse approaches from integer-order to fractional systems. Traditional models often focus on vaccinations (Rodrigues, Monteiro & Torres 2014) or multi-strain competition (Glover & White 2020) yet frequently assume instantaneous changes and constant populations. While Zhu, Lin and Zhang (2020) introduced spatial dimensions through partial differential equations to track geographical movement, they focused on non-locality in space rather than time.

Biological control research has explored *Wolbachia* bacteria (Zhang & Lui 2020) and predator-prey dynamics involving larval stages (Siddik, Abdullah & Ismail 2020), though these also rely on classical derivatives that overlook hereditary properties. To capture these memory and non-local effects, fractional-order derivatives are increasingly employed (Moore, Sirisubtawee & Koonprasert 2019). Although Al-Sulami et al. (2014) utilized the Caputo fractional derivative to introduce memory, its singular kernel presents mathematical challenges in modeling real-world heterogeneities, highlighting the need for more robust temporal frameworks.

This research introduces two primary novelties to address existing literature gaps. First, it integrates the ecological predator-prey mechanism (Siddik, Abdullah & Ismail 2020) with fractional calculus to demonstrate how system 'memory' influences biological control success. Second, it replaces the singular Caputo derivative (Al-Sulami et al. 2014) with the Caputo-Fabrizio (CF) fractional operator. This choice is justified by its non-local, non-singular nature and fading memory property (Caputo & Fabrizio 2015), which better reflects transmission patterns dependent on recent history.

The study explores how larval predator-prey interactions regulate the dengue transmission cycle. Through rigorous mathematical analysis, we establish a theoretical foundation for disease outcomes. Using real-world demographic and incidence data for parameter estimation, the paper numerically investigates intervention strategies like vector control and human recovery.

The rest of the paper is structured thus as follow: The next two sections contain model description and qualitative stability analysis. Subsequent two sections show implicit numerical scheme, simulations, and results. While last section concludes the work.

MODEL DESCRIPTION

Following the model in Siddik, Abdullah and Ismail (2020), we have

$$\begin{aligned}
\frac{dH_S}{dt} &= \pi_H + \gamma_H H_R - \beta_1 \varepsilon_1 c H_S V_I - \mu_H H_S,\\
\frac{dH_I}{dt} &= \beta_1 \varepsilon_1 c H_S V_I - (\alpha_H + \delta_H + \mu_H) H_I,\\
\frac{dH_R}{dt} &= \alpha_H H_I - (\gamma_H + \mu_H) H_R,\\
\frac{dP}{dt} &= \Lambda_P + k\gamma_L L P - (\pi_P + \mu_P) P,\\
\frac{dL}{dt} &= \Lambda_L - (\gamma_L P + \pi_V + \mu_L) L,\\
\frac{dV_S}{dt} &= \pi_V L - \beta_2 \varepsilon_2 c H_I V_S - \mu_V V_S,\\
\frac{dV_I}{dt} &= \beta_2 \varepsilon_2 c H_I V_S - \mu_V V_I.
\end{aligned} \tag{2.1}$$

All parameters and initial conditions are non-negative for all $t \geq 0$. The total human population at time t, denoted by $H(t)$, is divided into susceptible humans $H_S(t)$, infected humans $H_I(t)$, and recovered humans $H_R(t)$. Similarly, the total adult *Aedes aegypti* mosquito stage at time t, denoted by $V(t)$, is split into susceptible mosquitoes $V_S(t)$ and infected mosquitoes $V_I(t)$. The model also has two compartments at the larval stages: the larval stage of predatory mosquitoes $P(t)$ and the larval stage of *Aedes aegypti* mosquitoes $L(t)$. See Siddik, Abdullah and Ismail (2020) for detailed model description.

We extend the existing literature by reformulating Equation (2.1) as a system of fractional differential equations. This approach is adopted because many real-world phenomena, including disease dynamics, exhibit memory, historical or nonlocal characteristics that are challenging to capture using traditional integer-order derivatives (Moore, Sirisubtawee & Koonprasert 2019). The Caputo-Fabrizio derivative is employed for the fractional operator due to its nonlocal nature, singularity-free property, and capacity to model fading memory (Caputo & Fabrizio 2015). This choice is particularly suitable for human behavior, which is often influenced by recent experiences rather than distant past events, and displays a tendency to forget information over time. We have the following definition (Caputo & Fabrizio 2015):

Definition 2.1 For a given function $g \in H^1(a, b)$, $b > a$, the Caputo-Fabrizio (CF) fractional derivative is defined as

$$D_t^\theta g(t) = \frac{\mathbb{M}(\theta)}{1-\theta} \int_a^t g'(s) \exp\left[-\theta \frac{t-s}{1-\theta}\right] ds. \tag{2.2}$$

where $\mathbb{M}(\theta)$ is a normalization functions satisfying $\mathbb{M}(0) = \mathbb{M}(1) = 1$. $\theta \in (0,1)$. $\theta \in (0, 1)$ represents the fractional order index.

TABLE 1. Description of parameters

Parameter	Description	Value	Reference
π_H	Recruitment rate of human	$N_0\mu_H$	
π_V	Progression rate of larva to *Aedes aegypti* mosquitoes	1/7 day^{-1}	(Eco-friendly)
μ_H	Natural death of human	0.0059 $year^{-1}$	(Pop. of Mal.)
δ_H	Disease-induced death of human	4.89×10^{-6} day^{-1}	Fitted
γ_H	Human loss of immunity rate	0.02877 day^{-1}	(Siddik, Abdullah & Ismail 2020)
β	Transmission rate from infected vector to susceptible human	6.96×10^{-10} $mosquito^{-1}day^{-1}$	Fitted
ρ	Transmission rate from infected human to susceptible vector	4.39×10^{-9} $human^{-1}$ day^{-1}	Fitted
α_H	Recovery rate of human	0.1428 day^{-1}	(Al-Sulami et al. 2014)
μ_V	Natural death of *Aedes aegypti* mosquito	1/38 day^{-1}	(Brady et al. 2013)
Λ_P	Egg laying rate of predatory mosquitoes	1.2 larvae L^{-1} day^{-1}	Assumed
Λ_L	Egg laying rate of *Aedes aegypti* mosquitoes	20 larvae L^{-1} day^{-1}	Assumed
K	Tropical convention efficiency	0.1	(Ghosh, Lashari & Li 2013)
γ_L	Predation larva stage by predatory mosquitoes	8×10^{-4} L $larva^{-1}$ day^{-1}	Assumed
π_P	Larva stage of predatory mosquitoes	0.0625 day^{-1}	(Ghosh, Lashari & Li 2013)
μ_P	Natural death of predatory mosquitoes	1/21 day^{-1}	(Malla et al. 2023)
μ_L	Natural death of *Aedes aegypti* larva	0.05 day^{-1}	(Ghosh, Lashari & Li 2013)
ϖ	Volume of liquid habitat containing larvae that transition into mosquitoes	100000 L	Assumed

The dynamics of dengue virus transmission among humans, in the context of a predator-prey ecosystem, are described by the following system of fractional differential equations. Where, for notational convenience, we take $\beta = \beta_1\varepsilon_1 c$ and $\rho = \beta_2\varepsilon_2 c$. The larval population is measured in terms of larvae per liter of liquid, while the adult mosquito population is not quantified in such a manner. To ensure dimensional consistency, we introduce the parameter ϖ into sixth Equation in (2.3). This parameter represents the volume (in liters) of liquid habitat containing larvae that transition into adult mosquitoes, assuming that each larva develops into a single mosquito. This assumption simplifies the developmental process for modeling purposes and ensures coherence in the system's units. A detailed description of ϖ and other model parameters is provided in Table 1.

$$\begin{aligned}
D_t^\theta H_S &= \pi_H + \gamma_H H_R - \beta H_S V_I - \mu_H H_S,\\
D_t^\theta H_I &= \beta H_S V_I - (\alpha_H + \delta_H + \mu_H) H_I,\\
D_t^\theta H_R &= \alpha_H H_I - (\gamma_H + \mu_H) H_R,\\
D_t^\theta P &= \Lambda_P + k\gamma_L L P - (\pi_P + \mu_P) P,\\
D_t^\theta L &= \Lambda_L - (\gamma_L P + \pi_V + \mu_L) L,\\
D_t^\theta V_S &= \varpi\pi_V L - \rho H_I V_S - \mu_V V_S,\\
D_t^\theta V_I &= \rho H_I V_S - \mu_V V_I.
\end{aligned} \tag{2.3}$$

A dimensional inconsistency arises in model (2.3) as the right-hand side has units of day^{-1} while the fractional operator on the left has units of $day^{-\theta}$. To rectify this, we adopt the normalization approach outlined in Correa-Escudero et al. (2022), in which case the normalization parameter is taken as 1.

MODEL ANALYSIS

DISEASE-FREE EQUILIBRIUM

The disease-free equilibrium (DFE) represents a non-epidemic state where the disease is entirely absent from the population. Mathematically, the DFE is identified by setting all infected compartments to zero, resulting in a stable population unaffected by transmission:

$$\Pi_0 = (H_S^\star, H_I^\star, H_R^\star, P^\star, L^\star, V_S^\star, V_I^\star) = \left(\frac{\pi_H}{\mu_H}, 0, 0, P^\star, L^\star, \frac{\varpi \pi_V L^\star}{\mu_V}, 0\right),$$

where the values for P^* and L^* are given by:

$$P^\star = \frac{\gamma_L \Lambda_P + k\gamma_L \Lambda_L - (\pi_P + \mu_P)(\pi_V + \mu_L) + \sqrt{\eth}}{2\gamma_L(\pi_P + \mu_P)}, \quad (3.1)$$

$$L^\star = \frac{k\gamma_L \Lambda_L + \gamma_L \Lambda_P + (\pi_P + \mu_P)(\pi_V + \mu_L) - \sqrt{\eth}}{2k\gamma_L(\pi_V + \mu_L)}, \quad (3.2)$$

where $\eth = [\gamma_L \Lambda_P + k\gamma_L \Lambda_L - (\pi_P + \mu_P)(\pi_V + \mu_L)]^2 + 4\gamma_L \Lambda_P (\pi_P + \mu_P)(\pi_V + \mu_L)$.

The basic reproduction number, $\Re_0$, which indicates the average number of secondary infections generated by an infected individual in a partially susceptible population, is derived using the next-generation matrix approach:

$$\Re_0 = \frac{\beta \rho H_S^\star V_S^\star}{\mu_V(\alpha_H + \delta_H + \mu_H)}.$$

Theorem 3.1 The disease-free equilibrium Π_0 *of model* (2.3) *is globally asymptotically stable in* Θ *if* $\Re_0 < 1$ *and there exists* t_0 *such that* $L(t) < \frac{\pi_P + \mu_P}{k\gamma_L}$ *for* $t > t_0$.

To establish this theorem, we separate model 2.3 into two subsystems - predator-prey interaction subsystem and system without predator-prey interaction.

Predator-Prey Interaction Subsystem

The predator-prey interaction subsystem is represented as:

$$\begin{aligned} D_t^\theta P &= \Lambda_P + k\gamma_L LP - (\pi_P + \mu_P)P, \\ D_t^\theta L &= \Lambda_L - (\gamma_L P + \pi_V + \mu_L)L, \end{aligned} \quad (3.3)$$

where the equilibrium point (P^*, L^*) is shown by (3.1) and (3.2). The region of solution of (3.3) is obtained as

$$\Theta_1 = \left\{(P, L) \in \mathbb{R}_+^2 \middle| P \le \frac{\Lambda_P}{\pi_P + \mu_P}, L \le \frac{\Lambda_L}{\pi_V + \mu_L}\right\}.$$

Theorem 3.2 The equilibrium point (P^*, L^*) is shown by (3.1) and (3.2) is globally asymptotically stable in Θ_1 provided there exists t_0 such that $L(t) < \frac{\pi_P + \mu_P}{k\gamma_L}$ for $t > t_0$.

Proof We define a Lyapunov function

$$\mathscr{L} = \frac{L^\star}{2}(P - P^\star)^2 + \frac{kP^\star}{2}(L - L^\star)^2.$$

Taking the fractional derivative with respect to time, we have

$$\begin{aligned} D_t^\theta \mathscr{L} &= L^\star(P - P^\star) D_t^\theta P + kP^\star(L - L^\star) D_t^\theta L, \\ &= L^\star(P - P^\star)[\Lambda_P + k\gamma_L LP - (\pi_P + \mu_P)P] + kP^\star(L - L^\star)[\Lambda_L - (\gamma_L P + \pi_V + \mu_L)L]. \end{aligned}$$

At equilibrium,

$\Lambda_P = -k\gamma_L L^* P^* + (\pi_P + \mu_P) P^*$ and $\Lambda_L = \gamma_L P^* L^* - (\pi_V + \mu_L) L^*$,

therefore,

$$\begin{aligned} D_t^\theta \mathscr{L} &= -L^\star(\pi_P + \mu_P)(P - P^\star) + L^\star(P - P^\star)[k\gamma_L P^\star(L - L^\star) + k\gamma_L L(P - P^\star)] \\ &\quad - kP^\star(\pi_V + \mu_L)(L - L^\star) + kP^\star(L - L^\star)[-\gamma_L L^\star(P - P^\star) - \gamma_L P(L - L^\star)], \\ &= -L^\star(\pi_P + \mu_P - k\gamma_L L)(P - P^\star)^2 - kP^\star(\pi_V + \mu_L + \gamma_L P)(L - L^\star)^2. \end{aligned}$$

Since $L^\star < \frac{\pi_P + \mu_P}{k\gamma_L}$, we know that the term $\pi_P + \mu_P - k\gamma_L L^* > 0$, which implies that both terms in the expression for $D_t^\theta \mathscr{L}$ are non-positive. Consequently, we have:

$$D_t^\theta \mathscr{L} \le 0 \quad \text{for all } t \ge 0.$$

The non-increasing nature of the Lyapunov function L indicates that the system cannot diverge from the equilibrium point. Furthermore, since $D_t^\theta \mathscr{L} = 0$ when $P = P^*$ and $L = L^*$, it follows from LaSalle's invariance principle LaSalle that the equilibrium point (P^*, L^*) is globally asymptotically stable.

Model Without Predator-Prey Interaction

For a fixed $L = L^0$, the system simplifies to:

$$\begin{aligned} D_t^\theta H_S &= \pi_H + \gamma_H H_R - \beta H_S V_I - \mu_H H_S, \\ D_t^\theta H_I &= \beta H_S V_I - (\alpha_H + \delta_H + \mu_H) H_I, \\ D_t^\theta H_R &= \alpha_H H_I - (\gamma_H + \mu_H) H_R, \\ D_t^\theta V_S &= \varpi \pi_V L^0 - \rho V_S H_I - \mu_V V_S, \\ D_t^\theta V_I &= \rho V_S H_I - \mu_V V_I. \end{aligned} \quad (3.4)$$

The disease-free equilibrium point in this scenario is:

$$\chi_0 = \left(\frac{\pi_H}{\mu_H}, 0, 0, \frac{\varpi \pi_V L^0}{\mu_V}, 0\right),$$

the basic reproduction number is

$$\Re_0^1 = \frac{\beta \rho \pi_H \varpi \pi_V L^0}{\mu_H \mu_V^2 (\alpha_H + \delta_H + \mu_H)},$$

the solution region is given as

$$\Theta_2 = \left\{(H_S, H_I, H_R) \in \mathbb{R}_+^3, (V_S, V_I) \in \mathbb{R}_+^2 \middle| H = H_S + H_I + H_R \le \frac{\pi_H}{\mu_H}, V = V_S + V_I \le \frac{\omega \pi_V L^v}{\mu_V}\right\}.$$

Theorem 3.3 The disease-free equilibrium χ_0 *of* (3.4) *is globally asymptotically stable in* Θ_2 *if* $\mathcal{R}_0^1 < 1$.

Proof. We define a Lyapunov function

$$\mathfrak{L} = \frac{\rho V_S^\star + \mu_V}{\mu_V(\alpha_H + \delta_H + \mu_H)} H_I + \frac{\beta H_S^\star + \alpha_H + \delta_H + \mu_H}{\mu_V(\alpha_H + \delta_H + \mu_H)} V_I.$$

Taking the fractional derivative with respect to time, we have

$$\begin{aligned} D_t^\theta \mathfrak{L} &= \frac{\rho V_S^\star + \mu_V}{\mu_V(\alpha_H + \delta_H + \mu_H)} D_t^\theta H_I + \frac{\beta H_S^\star + \alpha_H + \delta_H + \mu_H}{\mu_V(\alpha_H + \delta_H + \mu_H)} D_t^\theta V_I, \\ &= \frac{\rho V_S^\star + \mu_V}{\mu_V(\alpha_H + \delta_H + \mu_H)} [\beta H_S V_I - (\alpha_H + \delta_H + \mu_H) H_I] \\ &\quad + \frac{\beta H_S^\star + \alpha_H + \delta_H + \mu_H}{\mu_V(\alpha_H + \delta_H + \mu_H)} [\rho V_S H_I - \mu_V V_I], \\ &= \left(\frac{\beta \rho H_S V_S^\star}{(\alpha_H + \delta_H + \mu_H)\mu_V} - \frac{\beta(H_S^\star - H_S)}{\alpha_H + \delta_H + \mu_H} - 1 \right) V_I \\ &\quad + \left(\frac{\beta \rho H_S^\star V_S}{(\alpha_H + \delta_H + \mu_H)\mu_V} - \frac{\rho(V_S^\star - V_S)}{\mu_V} - 1 \right) H_I, \\ &= (\mathfrak{R}_0 - 1)(H_I + V_I) - \frac{\beta(H_S^\star - H_S)V_I}{\alpha_H + \delta_H + \mu_H} \left(\frac{\rho V_S^\star}{\mu_H} + 1 \right) \\ &\quad - \frac{\rho(V_S^\star - V_S)H_I}{\mu_V} \left(\frac{\beta H_S^\star}{\alpha_H + \delta_H + \mu_H} + 1 \right). \end{aligned}$$

From these expression, it follows that $D_t^\theta \mathfrak{L} < 0$ when $\mathfrak{R}_0 < 1$. If R_0=1, then $D_t^\theta \mathfrak{L} = 0$ under the following conditions:

a) $H_I = V_I = 0$,
b) $H_I = 0$ and $H^*_S = H_S$,
c) $V_I = 0$ and $V^*_S = V_S$,
d) $H^*_S = H_S$ and $V^*_S = V_S$.

In all these cases, $D_t^\theta \mathfrak{L} = 0$ only at the disease-free equilibrium χ_0. By LaSalle's Invariance Principle, every trajectory of the model (3.4) converges to the largest compact invariant set within Γ, which is the disease-free equilibrium χ_0. Hence, χ_0 is globally asymptotically stable in Γ when $\mathfrak{R}_0 < 1$.

Theorem 3.1 follows from Theorems 3.2 & 3.3.

ENDEMIC EQUILIBRIUM

Provided $\mathfrak{R}_0^1 > 1$, the endemic equilibrium of the system (3.11) is derived as:

$$H_S^{\star\star} = \frac{\mu_V(\rho H_I^{\star\star} + \mu_V)(\pi_H \gamma_H + \pi_H \mu_H + \alpha_H \gamma_H H_I^{\star\star})}{(\gamma_H + \mu_H)[\beta \rho \varpi \pi_V L^0 H_I^{\star\star} + \mu_H \mu_V(\rho H_I^{\star\star} + \mu_V)]},$$

$$H_R^{\star\star} = \frac{\alpha_H H_I^{\star\star}}{\gamma_H + \mu_H}, \quad V_S^{\star\star} = \frac{\varpi \pi_V L^0}{\rho H_I^{\star\star} + \mu_V}, \quad V_I^{\star\star} = \frac{\rho \varpi \pi_V L^0 H_I^{\star\star}}{\mu_V(\rho H_I^{\star\star} + \mu_V)},$$

where

$$H_I^{\star\star} = \frac{(\gamma_H + \mu_H)(\alpha_H + \delta_H + \mu_H)\mu_H \mu_V^2 [\mathfrak{R}_0^1 - 1]}{\rho(\gamma_H + \mu_H)(\alpha_H + \delta_H + \mu_H)(\beta \varpi \pi_V L^0 + \mu_H \mu_V) - \beta \rho \varpi \pi_V \alpha_H \gamma_H L^0}.$$

The denominator is positive, ensuring the existence and uniqueness of the endemic equilibrium, provided $\mathfrak{R}_0^1 > 1$.

NUMERICAL SCHEME FOR (2.3)

Drawing inspiration from previous works (Adewole, Abdullah & Ali 2024; Atangana & Owolabi 2018; Owolabi 2018), we propose an implicit scheme for resolving the fractional differential Equation (2.3). The choice of an implicit scheme stems from its unconditional stability, making it an appropriate approach for this solution. Suppose we have

$$D_t^\theta S(t) = \chi_1(t, S(t)), \qquad S(0) = S_0, \quad \theta \in (0,1), \tag{4.1}$$

then

$$\frac{\mathbb{M}(\theta)}{1-\theta} \int_0^t S'(s) \exp\left[-\theta \frac{t-s}{1-\theta} \right] ds = \chi_1(t, S(t)),$$

differentiating both sides with respect to t,

$$\frac{\mathbb{M}(\theta)}{1-\theta} S'(t) - \frac{\theta}{1-\theta} \chi_1(t, S(t)) = \frac{d}{dt} \chi_1(t, S(t)),$$

it therefore follows that

$$S(t) = S(0) + \frac{1-\theta}{\mathbb{M}(\theta)} \chi_1(t, S(t)) + \frac{\theta}{\mathbb{M}(\theta)} \int_0^t \chi_1(s, S(s))\, ds.$$

At $t = t_j$ and $t = t_{j+1}$, $j = 0, 1, 2, \ldots$, we have

$$S(t_j) = S(0) + \frac{1-\theta}{\mathbb{M}(\theta)} \chi_1(t_j, S(t_j)) + \frac{\theta}{\mathbb{M}(\theta)} \int_0^{t_j} \chi_1(s, S(s))\, ds, \tag{4.2}$$

$$S(t_{j+1}) = S(0) + \frac{1-\theta}{\mathbb{M}(\theta)} \chi_1(t_{j+1}, S(t_{j+1})) + \frac{\theta}{\mathbb{M}(\theta)} \int_0^{t_{j+1}} \chi_1(s, S(s))\, ds, \tag{4.3}$$

respectively. Subtract (4.2) from (4.3),

$$S(t_{j+1}) - S(t_j) = \frac{1-\theta}{\mathbb{M}(\theta)} \left[\chi_1(t_{j+1}, S(t_{j+1})) - \chi_1(t_j, S(t_j)) \right] + \frac{\theta}{\mathbb{M}(\theta)} \int_{t_j}^{t_{j+1}} \chi_1(s, S(s))\, ds. \tag{4.4}$$

We approximate

$$\chi_1(t, S(t)) \approx \frac{t - t_{j+1}}{t_j - t_{j+1}} \chi_1(t_j, S(t_j)) + \frac{t - t_j}{t_{j+1} - t_j} \chi_1(t_{j+1}, S(t_{j+1})).$$

Take $h = t_{j+1} - t_j$, then

$$\chi_1(t, S(t)) \approx \frac{1}{h} \left[(t - t_j) \chi_1(t_{j+1}, S(t_{j+1})) - (t - t_{j+1}) \chi_1(t_j, S(t_j)) \right].$$

Thus,

$$\begin{aligned} \int_{t_j}^{t_{j+1}} \chi_1(s, S(s))\, ds &\approx \frac{1}{h} \left[\chi_1(t_{j+1}, S(t_{j+1})) \int_{t_j}^{t_{j+1}} (s - t_j)\, ds - \chi_1(t_j, S(t_j)) \int_{t_j}^{t_{j+1}} (s - t_{j+1})\, ds \right], \\ &= \frac{1}{h} \left[\chi_1(t_{j+1}, S(t_{j+1})) \frac{h^2}{2} + \chi_1(t_j, S(t_j)) \frac{h^2}{2} \right] = \frac{h}{2} \left[\chi_1(t_j, S(t_j)) + \chi_1(t_{j+1}, S(t_{j+1})) \right]. \end{aligned} \tag{4.5}$$

Substituting (4.5) into (4.4) yields

FIGURE 1. Trajectories of dengue transmission obtained from Clarke et al. (2024)

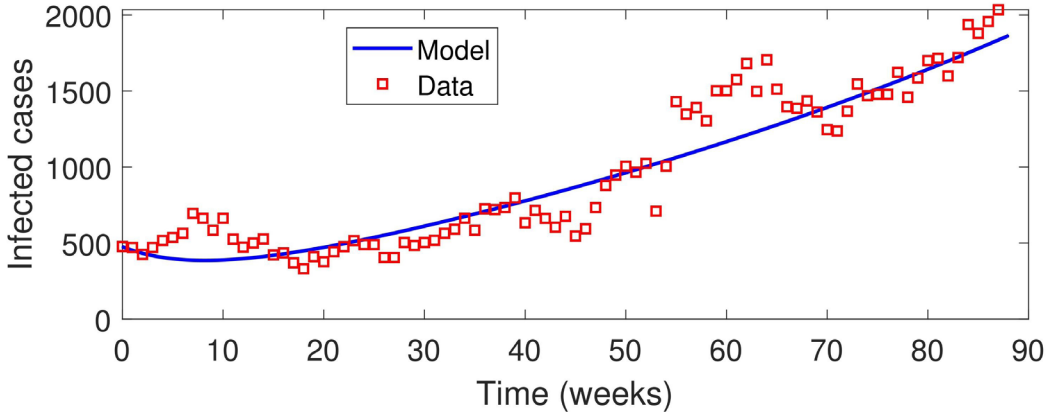

FIGURE 2. Model fitting

$$\begin{aligned} S(t_{j+1})-S(t_j) &= \frac{1-\theta}{\mathbb{M}(\theta)}\left[\chi_1(t_{j+1},S(t_{j+1}))-\chi_1(t_j,S(t_j))\right] \\ &\quad + \frac{\theta h}{2\mathbb{M}(\theta)}\left[\chi_1(t_j,S(t_j))+\chi_1(t_{j+1},S(t_{j+1}))\right], \\ &= \left(\frac{1-\theta}{\mathbb{M}(\theta)}+\frac{\theta h}{2\mathbb{M}(\theta)}\right)\chi_1(t_{j+1},S(t_{j+1})) \\ &\quad + \left(\frac{\theta h}{2\mathbb{M}(\theta)}-\frac{1-\theta}{\mathbb{M}(\theta)}\right)\chi_1(t_j,S(t_j)), \quad j=0,1,\ldots. \end{aligned} \tag{4.6}$$

The error produced by this method is presented in the Appendix.

SIMULATIONS AND DISCUSSION OF RESULTS

In this section, we implement the proposed scheme to simulate the model and investigate the infection dynamics. The numerical scheme is executed using MATLAB® codes while we take $\mathbb{M}(\theta) \equiv 1$.

PARAMETER ESTIMATION

For parameter estimation, the study uses the Open Dengue time series dataset (Clarke et al. 2024), specifically extracting weekly infection data from Malaysia. As shown in the data trajectory, Malaysia exhibited cyclic dengue patterns until August 2020, after which COVID-19 lockdown measures disrupted transmission; rates subsequently surged as restrictions were lifted. To maintain ecological realism despite limited field data, the model assumes a slow predatory egg-laying rate (1.2 eggs/liter daily) compared to the rapid reproduction of *Aedes aegypti* (20 eggs/liter daily). Furthermore, a low hunting rate is set to account for predator saturation and competition, while the liquid habitat volume (ϖ) is scaled to 100,000 liters to realistically represent aggregated urban breeding sites like drains and containers.

The model fitting focuses on the resurgence period from May 1, 2021 to December 31, 2022. Using a baseline human population of 33,000,000, initial conditions were set at $H_S(0)$ = 33, 000, 000 and $H_R(0)$ = 1000, with $H_I(0)$ derived from reported data and vector/predator populations assumed at $V_S(0) = 10^8$, $V_I(0)$ = 700, $L(0)$ = 100 and $P(0)$ = 10. The analysis estimates a fractional index (θ) of 0.211 and a basic reproduction number ($\Re_0$) of 1.441, with additional parameters detailed in Table 1.

The fractional index θ is integral to understanding the memory properties of the system. Lower values of θ correspond to stronger memory effects, where the system's current state is heavily influenced by its historical trajectory. The low fractional index $\theta = 0.211$ underscores strong memory effects, indicating that the dynamics of

dengue transmission are significantly shaped by historical factors, including prior mosquito populations, infection rates, and environmental conditions. This finding implies that changes or interventions in the system take time to reflect their full impact, emphasizing the need for sustained and comprehensive strategies to address both short-term and long-term drivers of dengue transmission.

To assess the goodness of fit, we employ the coefficient of determination (R^2), a widely accepted metric that quantifies how well a model captures the variability in observed data. The R^2-value ranges from 0 to 1, with higher values indicating a stronger fit. It is computed as:

$$R^2 = 1 - \frac{\sum(y_i - f_i)^2}{\sum(y_i - y_{av})^2}.$$

Here, y_i is the observed data value, y_{av} is the mean of the observed data, and f_i is the predicted value. For the fitted curve shown in Figure 2, the coefficient of determination is $R^2 = 0.889$, indicating a strong fit between the model and the observed data. This high R^2-value highlights the model's ability to accurately capture the underlying trends in dengue transmission. We take $\theta = 0.211$ in the subsequent simulations.

STABILITY AND BIFURCATION PLOTS

We conduct a numerical investigation to analyze the stability of the equilibrium point of system (3.9). The phase portrait of the system, presented in Figure 3, illustrates that the trajectories converge towards the equilibrium point irrespective of the initial values of P (predator population) and L (prey population). This convergence provides strong numerical evidence supporting the theoretical stability results established in Theorem 3.1. The observed behavior reaffirms the robustness of the equilibrium under varying initial conditions and highlights the system's tendency to reach a steady state over time.

Next, we analyze the bifurcation pattern of the model using β as the bifurcation parameter. Varying the value of β results in changes to both the basic reproduction number $\mathfrak{R}_0$ and the stationary solution of H_I (denoted as H^{**}). Figure 4 illustrates a forward bifurcation, indicating that the stationary solution of the infection compartment becomes zero whenever $\mathfrak{R}_0 \leq 1$. This demonstrates that the condition $\mathfrak{R}_0 < 1$ is sufficient for disease control, as no sustained infection is observed in this regime. Furthermore, this result aligns with the conclusions of Theorem 3.1, affirming the global stability of the disease-free equilibrium when $\mathfrak{R}_0 < 1$.

IMPACT OF PREDATOR-PREY INTERACTION ON THE DYNAMICS OF DENGUE

To investigate the impact of predator-prey interaction on the dynamics of dengue, we plot graphs that demonstrate how changes in predator (P) and prey (L) populations influence dengue dynamics. For this, we vary the egg-laying rate of predatory mosquitoes (Λ_P) and we observe changes in the stationary values of the predator population (P), prey population (L), the infected human compartment (H_I), and the basic reproduction number ($\mathfrak{R}_0$). To explore the effect of higher predator densities on infection dynamics, we plot the stationary values of L, H_I, and $\mathfrak{R}_0$ against the stationary value of P. The results are presented in Figure 5.

Figure 5 demonstrates an approximately linear relationship between increased predator density and declining mosquito larvae, which subsequently reduces the basic reproduction number ($\mathfrak{R}_0$) and infected human populations (H_I). However, ecological constraints like space and resource competition prevent predators from increasing indefinitely, meaning predation suppresses but rarely eradicates the disease.

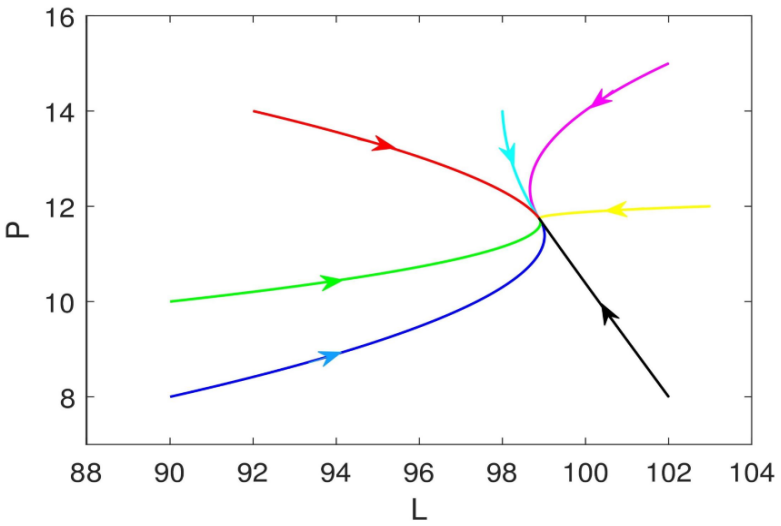

FIGURE 3. Phase portrait of the system (3.9) illustrating the stability of the equilibrium point

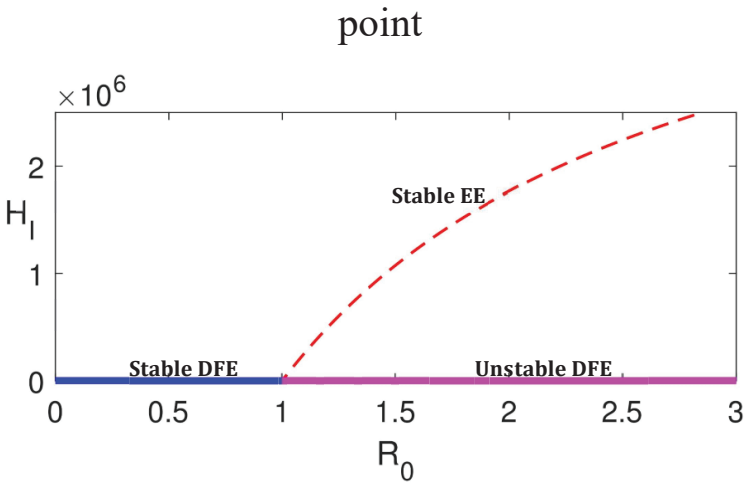

FIGURE 4. Bifurcation plot

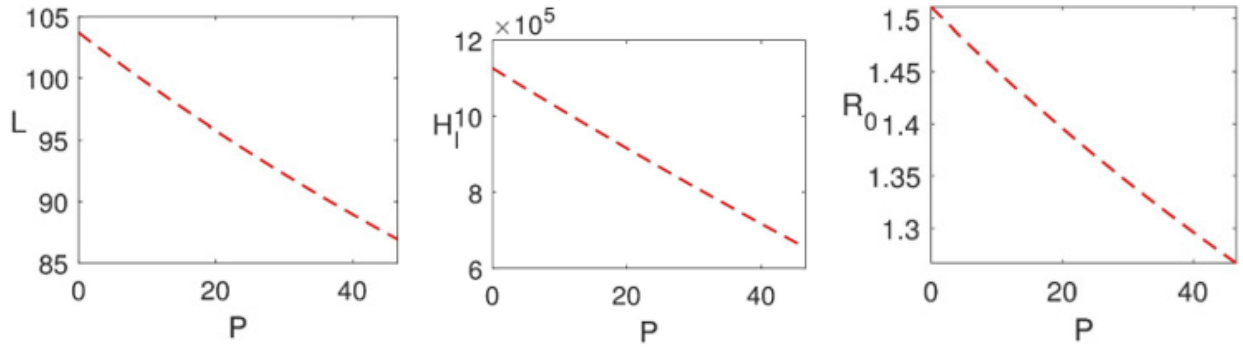

(a) (b) (c)

FIGURE 5. The relationship between predator density (P) and the stationary values of mosquito larvae (L), infected humans (H_I), and the basic reproduction number ($\mathfrak{R}_0$)

As shown in Figure 6, increasing predators from 10 to 50 per liter only modestly reduces larval density (from 103 to 101). This limited impact is driven by the high egg-laying rate (r_l) of *Aedes aegypti*, which maintains a baseline population. Additionally, predator saturation and functional response limits - such as reduced efficiency and intra-species competition at high densities - result in diminishing returns. Ultimately, high reproductive rates counteract predation pressure, sustaining a larval baseline despite significant predator increases.

Figure 6 illustrates that susceptible and infected adult mosquito populations remain relatively stable despite substantial increases in predator density. This stability occurs because predators primarily target the larval stage (L), and the transition from larvae to adults provides a continuous recruitment of the vector population. The high egg-laying rate (Λ_L) further ensures that a baseline number of larvae always mature into adults, counteracting predation pressure. The model's fractional-order nature introduces memory effects that create a temporal lag, moderating how quickly adult populations respond to larval reductions. Additionally, since disease parameters like the force of infection and recovery rates are independent of predator density, the infected mosquito and human populations experience only marginal changes.

Ultimately, while predator-prey interaction is a valuable control mechanism, it cannot achieve disease eradication alone. The residual larval population is sufficient to sustain transmission, suggesting that biological control must be integrated with additional measures for comprehensive dengue management.

SENSITIVITY ANALYSIS

Sensitivity analysis is a critical tool for evaluating how individual parameters drive infection dynamics (Saltelli et al. 2008). This study employs Latin Hypercube Sampling with Partial Rank Correlation Coefficient (LHS-PRCC) to quantify parameter influence on the basic reproduction number ($\mathfrak{R}_0$) and the stationary infected human population (H_I^{**}). This method identifies influential parameters whose uncertainties significantly impact prediction errors, ranking

them by relative importance (Blower & Dowlatabadi 1994; Hoops et al. 2016; Marino et al. 2008).

For uncertainty analysis, 5000 samples were generated across a range 50% above and below base values. Results in Figure 7 and Table 2 show that human-to-vector transmission (ρ) has the strongest positive correlation (PRCC = 0.9064), while vector-to-human transmission (β) also significantly elevates $\mathfrak{R}_0$ (PRCC = 0.6368). Similarly, the egg-laying rate (Λ_L) and larval progression rate (π_V) positively contribute to disease spread. Conversely, the human recovery rate (γ_h) and the natural mosquito death rate (μ_v = −0.8606) show strong negative correlations. These findings highlight that increasing human recovery or vector mortality are the most effective levers for reducing $\mathfrak{R}_0$.

The sensitivity analysis highlights that while the predatory mosquito egg-laying rate (Λ_P) is statistically significant, its low PRCC value indicates a relatively weak influence on disease dynamics compared to other factors. This suggests that while ecological interventions are beneficial for shaping vector populations, they are insufficient as standalone strategies. Other parameters, such as the human disease-induced death rate (δ_H), immunity loss rate (γ_H), and various predator-specific rates (γ_L, μ_P, π_P), show negligible correlations with the basic reproduction number ($\mathfrak{R}_0$). Consequently, the most effective interventions for controlling the initial outbreak involve targeting transmission rates (β, ρ), human recovery (α_H), and vector mortality (μ_V).

When analyzing the stationary infected human population (H_I^{**}), transmission rates (β), vector mortality (μ_V), and human recovery (α_H) remain critical, confirming their importance in both short-term and long-term dynamics. However, distinct differences emerge: the human-to-vector transmission rate (ρ), which heavily drives $\mathfrak{R}_0$, becomes negligible for H_I^{**}. Conversely, the human immunity loss rate (γ_H) shifts from negligible to a major positive driver of long-term prevalence. Additionally, δ_H exhibits a slightly more pronounced negative effect on the stationary state than it does on the initial spread.

In conclusion, parameters affecting $\mathfrak{R}_0$ primarily dictate early epidemic spread, whereas those impacting H_I^{**} determine the system's long-term equilibrium. While transmission and vector population size are key for initial control, mortality, recovery, and immunity loss are more significant for managing the steady-state infected population. Effective disease management should prioritize multi-faceted strategies - such as promoting human recovery, increasing vector mortality, and reducing immunity loss - to address both the immediate outbreak and the long-term disease burden.

SUGGESTED CONTROL STRATEGIES

Based on the sensitivity analysis, which highlighted the influence of various parameters on both the basic reproduction number ($\mathfrak{R}_0$) and the stationary infected human population (H_I^{**}), several targeted control strategies can be suggested:

Transmission control

This strategy focuses on reducing both the vector-to-human (β) and human-to-vector (ρ) transmission rates, which are key drivers of the basic reproduction number $\mathfrak{R}_0$. Since β and ρ represent distinct but interconnected transmission pathways, effective dengue control requires multifaceted interventions capable of disrupting transmission in both directions. In practice, many public health interventions, such as insecticide-treated mosquito nets, repellents, indoor residual spraying, and community-based environmental management, simultaneously reduce human exposure to infected mosquitoes and mosquito exposure to infected humans. In this sense, reductions in β and ρ are not independent parameter manipulations but reflect the combined impact of synergistic control measures.

Transmission control therefore encompasses personal protection strategies, including the use of insecticide-treated nets, repellents, and protective clothing, alongside public health education aimed at promoting early healthcare seeking, reduced human–mosquito contact, and sustained community engagement. To examine how these interventions affect dengue dynamics, we investigate the impact of reducing β and ρ on disease transmission.

Specifically, three scenarios are considered (Figure 8): reducing β alone by half while keeping ρ constant, reducing ρ alone by half while keeping β constant, and a combined scenario in which both β and ρ are simultaneously reduced to (β, ρ)/2. The combined scenario is designed to represent synergistic interventions that act on both transmission routes rather than isolated behavioral changes. In all three cases, the basic reproduction number is reduced to $\mathfrak{R}_0$ = 0.7205, with only minor quantitative differences in the outcomes.

The results show that reducing β alone leads to a more rapid decline in the infected human population (H_I), whereas reducing ρ alone accelerates the reduction in the infected vector population (V_I). The combined reduction of both β and ρ produces a balanced suppression of infection in both human and mosquito populations. Importantly, this outcome reflects the joint effect of interventions that simultaneously limit mosquito-to-human transmission and human-to-mosquito transmission, rather than an artificial redistribution of responsibility between population groups.

While reducing β alone places a strong burden on susceptible individuals through stringent personal protection requirements, the combined reduction scenario reflects more realistic public health practice, where responsibility is shared across the population through integrated interventions. This synergistic approach achieves effective and sustainable dengue control by weakening transmission in both directions of the infection cycle, making it more practical and robust than strategies targeting a single transmission pathway.

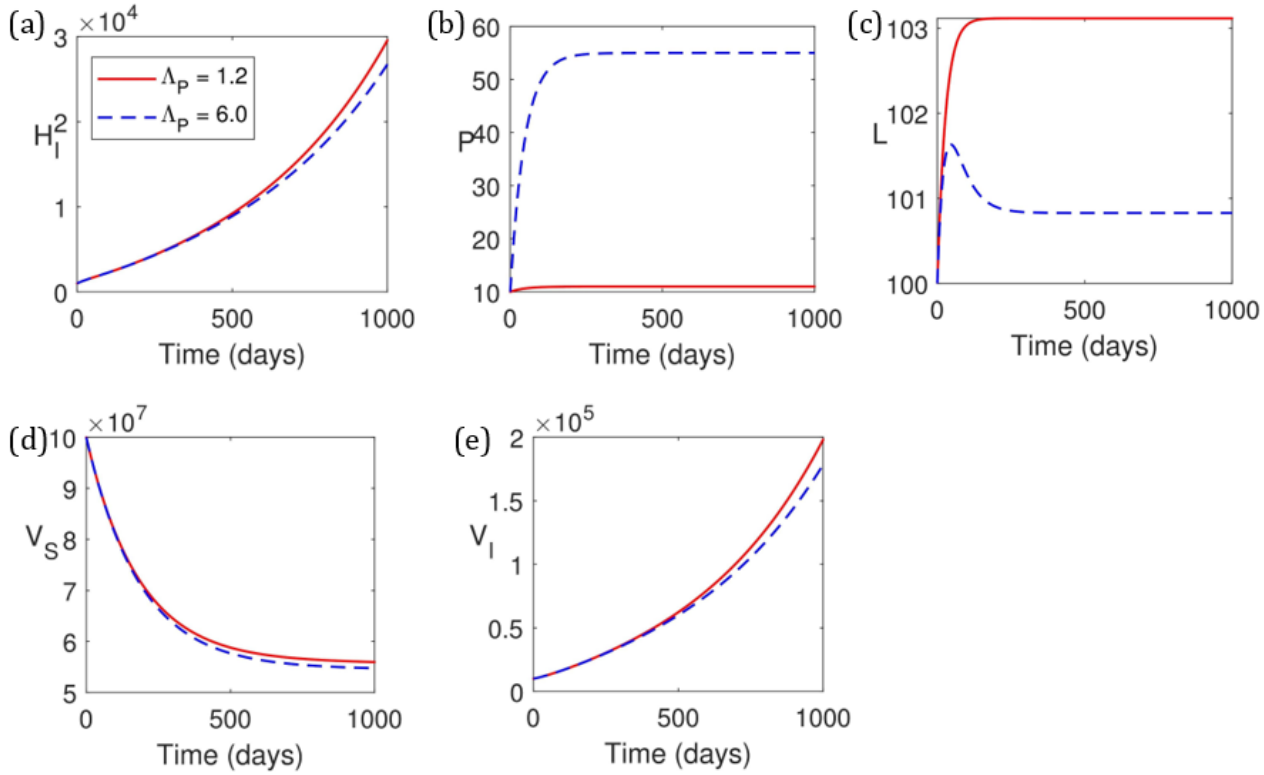

FIGURE 6. Impact of predator density (P) on the dynamics of dengue

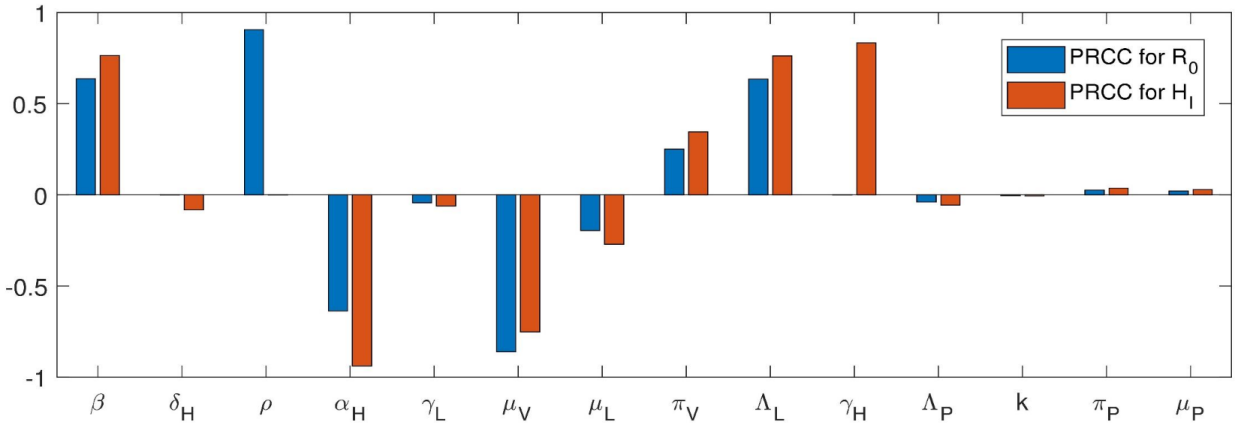

FIGURE 7. Partial Rank Correlation Coefficient (PRCC) values for model parameters with respect to ($\mathfrak{R}_0$) and H_I^{**}

Controlling vector populations

Effective vector control requires a multifaceted approach targeting the mosquito lifecycle. Measures such as larval source management and environmental interventions - including stagnant water removal and improved drainage - directly reduce the larval progression rate (π_v). Techniques like the Sterile Insect Technique (SIT) aim to lower the egg-laying rate (Λ_L) by releasing sterile males (Bourtzis & Vreysen 2021). Additionally, targeted insecticides like indoor residual spraying increase the adult death rate (μ_v). While biological control via natural predators offers a sustainable supplement, integrated strategies are essential for long-term suppression.

In practice, insecticide application is often spatially limited to human-populated zones, allowing mosquitoes from untreated areas to migrate and continue transmission. Our analysis shows that increasing μ_v by 50% reduces the basic reproduction number to $\mathfrak{R}_0$ = 0.6404$, highlighting the necessity of comprehensive coverage. Conversely, focusing on reproductive capacity through SIT has seen global success, such as in Havana, Cuba, where field trials achieved complete population suppression of *Aedes*

TABLE 2. p-values for model parameters with respect to $\mathfrak{R}_0$ and H_I^{**}

	β	δ_H	ρ	α_H	γ_L	μ_V	μ_L	π_V	Λ_L	γ_H	Λ_P	k	π_P	μ_P
$\mathfrak{R}_0$	0	0.501	0	0	0.029	0	0	0	0	0.499	0.046	0.485	0.170	0.262
H^{**}	0	3.57×10^{-5}	0.499	0	0.002	0	0	0	0	0	0.005	0.472	0.059	0.135

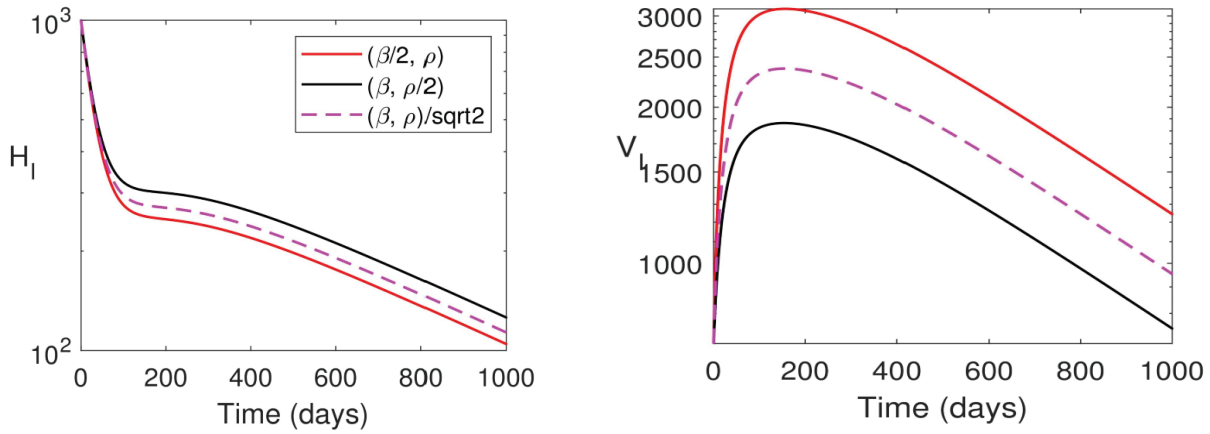

FIGURE 8. Time series plot investigating transmission control

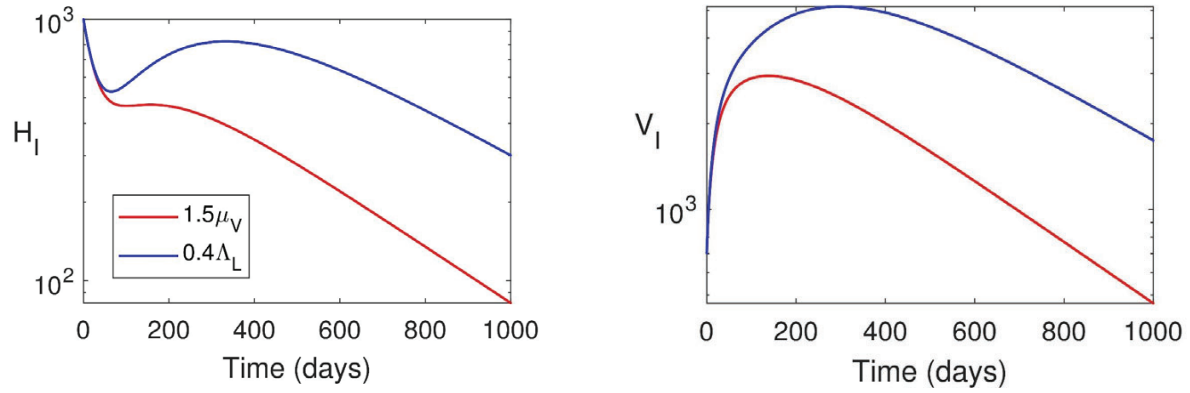

FIGURE 9. Time series plot investigating controlling vector populations

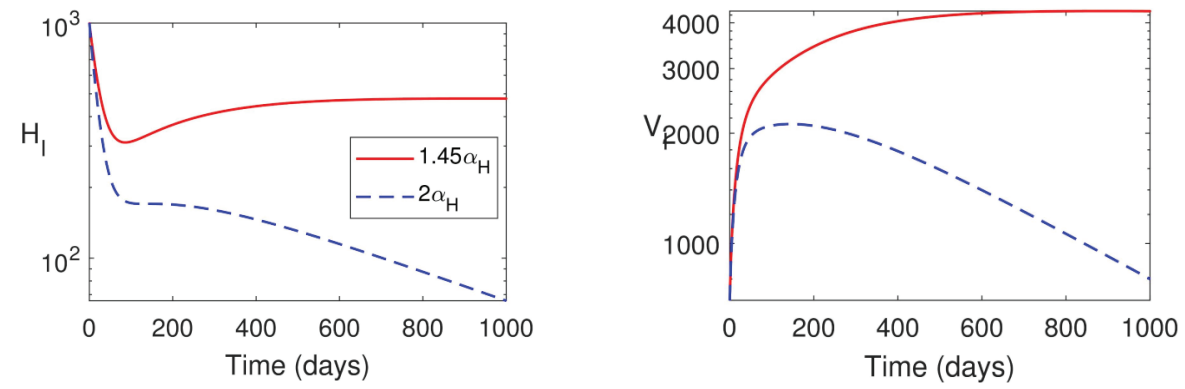

FIGURE 10. Time series plot investigating enhanced recovery rate

aegypti (Bourtzis & Vreysen 2021). Reducing Λ_L by 60% in our model results in a lower $\Re_0 = 0.5776$.

Despite the lower $\Re_0$ achieved by targeting Λ_L, interventions increasing μ_v (Figure 9) produce more immediate effects on dengue dynamics. This disparity exists because increasing the death rate directly impacts the current adult vector population. In contrast, reducing the egg-laying rate through SIT or larval control primarily affects the birth of future generations, creating a temporal lag before the impact manifests in the adult population responsible for transmission.

Enhancing human recovery

Enhancing the human recovery rate (α_H) is a critical strategy in controlling disease transmission and mitigating the long-term effects of infections. Early diagnosis, prompt access to effective treatment, and efficient healthcare interventions can significantly boost recovery rates, shorten the infectious period, and reduce both the basic reproduction number ($\Re_0$) and the steady-state infected human population (H_I^{**}). In this study, we explore the scenario where the recovery rate is improved by 45%, reflecting advancements in healthcare and treatment systems. This choice balances realistic expectations with empirical evidence, making it both significant and achievable.

Healthcare improvements, such as better diagnostic tools, faster access to medical care, and optimized treatment protocols, often yield noticeable reductions in recovery time. While a 100% improvement is overly optimistic, a 45% improvement represents a meaningful and realistic outcome. Empirical studies and data from regions with robust healthcare advancements report recovery time reductions ranging from 23.9% to 56.5% (Gyani et al. 2013), situating a 45% improvement well within plausible bounds. Moreover, sensitivity analyses show that α_H has a more pronounced effect on H_I^{**} than on $\Re_0$, as demonstrated by the simulation results in Figure 10. Specifically, a 45% increase in the recovery rate leads to $\Re_0 = 0.9938$, indicating that the disease is expected to vanish from the population. However, the decline is gradual, owing to the greater influence of α_H on H_I^{**} compared to $\Re_0$.

CONCLUSION

This research develops a fractional-order differential equation model to describe dengue dynamics, uniquely incorporating predator-prey interactions between predatory mosquitoes and larvae. By employing the Caputo-Fabrizio (CF) operator, the model captures 'fading memory', where recent events influence infection dynamics more than the distant past. Mathematical analysis confirms the model's reliability through positivity, boundedness, and stability. The disease-free equilibrium is stable when $\Re_0 < 1$, and numerical analysis confirms a forward bifurcation, suggesting that reducing $\Re_0$ below unity is sufficient for eradication.

An implicit numerical scheme was proposed, outperforming the traditional Adams-Bashforth method. Fitting the model to real-world data yielded a strong coefficient of determination ($R^2 = 0.889$) and a fractional-order index of 0.211. This low index indicates significant memory effects, implying that the impact of interventions on infection dynamics may manifest with a temporal lag. While increasing predator density successfully lowers $\Re_0$ and human infections, predation alone cannot eradicate the disease due to high larval influx, predator saturation, and resource competition.

Sensitivity analysis identified transmission rates (β, ρ), vector mortality (μ_v), and human recovery (a_H) as the most influential parameters. Reducing transmission and increasing mortality are critical for controlling the initial spread, while enhancing human recovery by 45% significantly reduces long-term prevalence. Consequently, the study recommends an Integrated Vector Management (IVM) approach, combining biological predators with chemical insecticides, environmental modifications, and the Sterile Insect Technique (SIT).

Policy recommendations emphasize reducing transmission via insecticide-treated materials and public awareness, alongside strengthening healthcare for early diagnosis. Because of the identified memory effects, policymakers must adopt long-term, adaptive strategies rather than expecting immediate results. Although limited by assumptions of homogeneous mixing and the exclusion of imported cases, this work provides a robust framework for public health specialists, highlighting that sustainable dengue management requires a multifaceted integration of ecological, medical, and social interventions.

ACKNOWLEDGEMENTS

This research is funded by a collaboration between Universiti Malaysia Perlis (UniMAP) and Hasanuddin University (UNHAS) through the International Research Fund (INTERES) year 2024. During the preparation of this work, we used ChatGPT in order to improve the language. After using this AI tool, we reviewed and edited the content as needed and take full responsibility for the content of the publication. We have no competing interests to declare that are relevant to the content of this article.

REFERENCES

Abuteen, E. 2024. Solving fractional riccati differential equation with caputo-fabrizio fractional derivative. European. *Journal of Pure and Applied Mathematics* 17(1):372–384.

Adewole, M.O., Abdullah, F.A. & Ali, M.K.M. 2024. Dynamics of leptospirosis in human and rodent populations: A multiscale modeling approach. *Journal of Biological Systems* 32(2): 605-641.

Al-Sulami, H., El-Shahed, M., Nieto, J.J. & Shammakh, W. 2014. On fractional order dengue epidemic model. *Mathematical Problems in Engineering* 6: 456537.

Atangana, A. & Owolabi, K.M. 2018. New numerical approach for fractional differential equations. *Mathematical Modelling of Natural Phenomena* 13(1): Paper No. 3, 21.

Blower, S.M. & Dowlatabadi, H. 1994. Sensitivity and uncertainty analysis of complex models of disease transmission - An HIV model as an example. *International Statistical Review* 62: 229-243.

Bourtzis, K. & Vreysen, M.J.B. 2021. Sterile insect technique (SIT) and its applications. *Insects* 12(7): 638.

Brady, O.J., Johansson, M.A., Guerra, C.A., Bhatt, S., Golding, N., Pigott, D.M., Delatte, H., Grech, M.G., Leisnham, P.T., Maciel-de Freitas, R., Styer, L.M., Smith, D.L., Scott, T.W., Gething, P.W. & Hay, S.I. 2013. Modelling adult *Aedes aegypti* and *Aedes albopictus* survival at different temperatures in laboratory and field settings. *Parasites & Vectors* 6: 351.

Caputo, M. & Fabrizio, M. 2015. A new definition of fractional derivative without singular kernel. *Progress in Fractional Differentiation and Applications* 1(2): 73-85.

Clarke, J., Lim, A., Gupte, P., Pigott, D.M., van Panhuis, W.G. & Brady, O.J. 2024. A global dataset of publicly available dengue case count data. *Scientific Data* 11(1): 296.

Correa-Escudero, I.L., Gomez-Aguilar, J.F., López-López, M.G., Alvarado-Martínez, V.M. & Baleanu, D. 2022. Correcting dimensional mismatch in fractional models with power, exponential and proportional kernel: Application to electrical systems. *Results in Physics* 40: 105867.

Charette, M., Berrang-Ford, L., Llanos-Cuentas, E.A., Cárcamo, C. & Kulkarni, M. 2017. What caused the 2012 dengue outbreak in Pucallpa, Peru? A socio-ecological autopsy. *Social Science & Medicine* 174: 122-132.

Cui, Z. 2022. Solutions of some typical nonlinear differential equations with Caputo-Fabrizio fractional derivative. *AIMS Math* 7(8): 14139-14153.

Ghosh, M., Lashari, A.A. & Li, X.Z. 2013. Biological control of malaria: A mathematical model. *Applied Mathematics and Computation* 219(15): 7923-7939.

Glover, A. & White, A. 2020. A vector-host model to assess the impact of superinfection exclusion on vaccination strategies using dengue and yellow fever as case studies. *Journal of Theoretical Biology* 484: 110014.

Gutiérrez-Barbosa, H., Castañeda, N. Y. & Castellanos, J. E. 2019. Differential replicative itness of the four dengue virus serotypes circulating in Colombia in human liver Huh7 cells. *The Brazilian Journal of Infectious Diseases*. In press, corrected proof, Available online 13 December 2019.

Guzman, M.G., Halstead, S.B., Artsob, H., Buchy, P., Farrar, J., Gubler, D.J., Hunsperger, E., Kroeger, A., Margolis, H.S., Martínez, E., Nathan, M.B., Pelegrino, J.L., Simmons, C., Yoksan, S. & Peeling, R.W. 2010. Dengue: A continuing global threat. *Nat. Rev. Microbiol.* 8(12 Suppl): S7-16. doi: 10.1038/nrmicro2460

Gyani, A., Shafran, R., Layard, R. & Clark, D.M. 2013. Enhancing recovery rates: Lessons from year one of IAPT. *Behaviour Research and Therapy* 51(9): 597-606.

Hoops, S., Hontecillas, R., Abedi, V., Leber, A., Philipson, C., Carbo, A. & Bassaganya-Riera, J. 2016. Ordinary differential equations (ODEs) based modeling. In *Computational Immunology: Models and Tools*, Chapter 5, Elsevier. pp. 63-78.

Malla, R.K., Mandal, K.K., Burman, S., Das, S., Ghosh, A. & Chandra, G. 2023. Numerical analysis of predatory potentiality of *Toxorhynchites splendens* against larval *Aedes albopictus* in laboratory and semi-field conditions. *Scientific Reports* 13(1): 7403.

Marino, S., Hogue, I.B., Ray, C.J. & Kirschner, D.E. 2008. A methodology for performing global uncertainty and sensitivity analysis in systems biology. *Journal of Theoretical Biology* 254(1): 178-196.

Moore, E.J., Sirisubtawee, S. & Koonprasert, S. 2019. A Caputo-Fabrizio fractional differential equation model for HIV/AIDS with treatment compartment. *Advances in Difference Equations* 20: Paper No. 200.

Owolabi, K.M. 2018. Numerical patterns in reaction-diffusion system with the Caputo and Atangana-Baleanu fractional derivatives. *Chaos, Solitons & Fractals* 115: 160-169.

Rodrigues, H.S., Monteiro, M.T.T. & Torres, D.F.M. 2014. Vaccination models and optimal control strategies to dengue. *Mathematical Biosciences* 247: 1-12.

Saltelli, A., Ratto, M., Andres, T., Campolongo, F., Cariboni, J., Gatelli, D., Saisana, M. & Tarantola, S. 2008. *Global Sensitivity Analysis: The Primer*. Chichester: John Wiley & Sons.

Siddik, S.B.M., Abdullah, F.A. & Ismail, A.I.M. 2020. Mathematical model of dengue virus with predator-prey interactions. *Sains Malaysiana* 49(5): 1191-1200.

Srivastav, A.K. & Ghosh, M. 2019. Assessing the impact of treatment on the dynamics of dengue fever: A case study of India. *Applied Mathematics and Computation* 362: 124533.

World Health Organization. 2018. WHO 2016. Dengue report 2018. URL:http://www.who.int/dengue/publications/world_dengue_report_2018/report/en.

Zhang, H. & Lui, R. 2020. Releasing Wolbachia-infected *Aedes aegypti* to prevent the spread of dengue virus: A Mathematical study. *Infectious Disease Modelling* 5: 142-160.

Zhu, M., Lin, Z. & Zhang, L. 2020. Spatial-temporal risk index and transmission of a nonlocal dengue model. *Nonlinear Analysis: Real World Applications* 53: 103076.

*Corresponding author; email: olamatthews@ymail.com

APPENDIX

NUMERICAL SCHEME

NUMERICAL EXPERIMENT TO CHECK THE ACCURACY OF THE PROPOSED SCHEME

Example 6.1. Consider the following fractional logistic differential equation

$$D_t^{\theta}U(t) = U(t) - U^2(t), \qquad U(0) = \frac{1}{2},\ t \geq 0,\ \theta \in (0,1),\ \mathbb{M}(\theta) \equiv 1. \tag{6.1}$$

The exact solution is given as (Abuteen 2024)

$$|U|^{\theta}|1-U|^{\theta-2} = 2^{2-2\theta}e^{\theta t}$$

We solve (6.1) using the proposed scheme as well as the two-step Adams–Bashforth scheme (ABS) (Atangana & Owolabi 2018). From (4.6),

$$U_{j+1} = U_j + (1-\theta)\left(U_{j+1} - U_{j+1}^2 - U_j + U_j^2\right) + \frac{\theta h}{2}\left(U_j - U_j^2 + U_{j+1} - U_{j+1}^2\right).$$

This leads to

$$U_{j+1} = \frac{U_j + (1-\theta)\left(-U_j + U_j^2\right) + \frac{\theta h}{2}\left(U_j - U_j^2\right)}{1 - \left(1 - \theta + \frac{\theta h}{2}\right)\left(1 - U_{j+1}\right)}.$$

Linearizing

$$U_{j+1} = \frac{U_j + (1-\theta)\left(-U_j + U_j^2\right) + \frac{\theta h}{2}\left(U_j - U_j^2\right)}{\left[1 - \left(1 - \theta + \frac{\theta h}{2}\right)\left(1 - \left(2U_j - U_{j-1}\right)\right)\right]}, \qquad j = 1,2,\ldots. \tag{6.2}$$

(6.2) is not self-starting, thus we obtain U_1 using

$$U_1 = \frac{U_0 + (1-\theta)\left(-U_0 + U_0^2\right) + \frac{\theta h}{2}\left(U_0 - U_0^2\right)}{\left[1 - \left(1 - \theta + \frac{\theta h}{2}\right)\left(1 - U_0\right)\right]}.$$

The solutions are presented in Tables 3-4 while the absolute relative error is defined as

$$\text{ARE} = \left|\frac{U_{\text{exact}} - U_{\text{approx}}}{U_{\text{exact}}}\right|.$$

Example 6.2. Consider the following fractional logistic differential equation

$$D_t^{\theta}Y(t) = Y(t)\left(1 - Y^2(t)\right), \qquad Y(0) = \frac{\sqrt{2}}{2},\ t \geq 0,\ \theta \in (0,1),\ \mathbb{M}(\theta) \equiv 1. \tag{6.3}$$

The exact solution is given as (Cui 2022)

$$|Y^2 - 1|^{2\theta-2}|Y|^{2\theta} = 2^{3-3\theta}e^{2\theta t}.$$

TABLE 3. Error estimates when $\theta = 0.7$

t	$h = 0.4$		$h = 0.2$		$h = 0.1$	
	PS	ABS	PS	ABS	PS	ABS
0	0	0	0	0	0	0
0.4	3.800×10^{-2}	3.800×10^{-2}	9.890×10^{-3}	1.556×10^{-2}	4.704×10^{-3}	7.095×10^{-3}
0.8	1.589×10^{-2}	3.560×10^{-2}	7.815×10^{-3}	1.537×10^{-2}	3.463×10^{-3}	6.984×10^{-3}
1.2	1.507×10^{-2}	3.543×10^{-2}	5.409×10^{-3}	1.473×10^{-2}	2.376×10^{-3}	6.688×10^{-3}
1.6	8.065×10^{-3}	3.262×10^{-2}	3.395×10^{-3}	1.391×10^{-2}	1.480×10^{-3}	6.314×10^{-3}
2.0	5.039×10^{-3}	3.112×10^{-2}	1.809×10^{-3}	1.308×10^{-2}	7.730×10^{-4}	5.932×10^{-3}

TABLE 4. Error estimates when $\theta = 0.5$

t	$h = 0.4$		$h = 0.2$		$h = 0.1$	
	PS	ABS	PS	ABS	PS	ABS
0	0	0	0	0	0	0
0.4	4.151×10^{-2}	4.151×10^{-2}	9.391×10^{-3}	1.832×10^{-2}	5.324×10^{-3}	8.654×10^{-3}
0.8	1.392×10^{-2}	3.873×10^{-2}	8.862×10^{-3}	1.735×10^{-2}	4.321×10^{-3}	8.195×10^{-3}
1.2	2.013×10^{-2}	3.969×10^{-2}	7.114×10^{-3}	1.598×10^{-2}	3.353×10^{-3}	7.560×10^{-3}
1.6	1.055×10^{-2}	3.657×10^{-2}	5.420×10^{-3}	1.443×10^{-2}	2.529×10^{-3}	6.835×10^{-3}
2.0	1.028×10^{-2}	3.627×10^{-2}	3.966×10^{-3}	1.281×10^{-2}	1.839×10^{-3}	6.080×10^{-3}

We solve (6.3) using the proposed scheme as well as the two-step Adams–Bashforth scheme (ABS) (Atangana & Owolabi 2018). From (4.6),

$$Y_{j+1} = Y_j + (1-\theta)\left(Y_{j+1}(1-Y_{j+1}^2) - Y_j(1-Y_j^2)\right) + \frac{\theta h}{2}\left(Y_j(1-Y_j^2) + Y_{j+1}(1-Y_{j+1}^2)\right).$$

This leads to

$$Y_{j+1} = \frac{-\theta(1-\frac{h}{2}) + \sqrt{4\left(1-\theta+\frac{\theta h}{2}\right)\left[Y_j + (\frac{\theta h}{2}-1+\theta)Y_j\left(1-Y_j^2\right)\right]Y_{j+1} + \theta^2(1-\frac{h}{2})^2}}{(1-\theta+\frac{\theta h}{2})Y_{j+1}}.$$

Linearizing, we obtain

$$Y_{j+1} = \frac{-\theta(1-\frac{h}{2}) + \sqrt{4\left(1-\theta+\frac{\theta h}{2}\right)\left[Y_j + (\frac{\theta h}{2}-1+\theta)Y_j\left(1-Y_j^2\right)\right](2Y_j - Y_{j-1}) + \theta^2(1-\frac{h}{2})^2}}{(1-\theta+\frac{\theta h}{2})(2Y_j - Y_{j-1})}. \quad (6.4)$$

(6.4) is not self-starting, thus we obtain U_1 using

$$Y_{j+1} = \frac{-\theta(1-\frac{h}{2}) + \sqrt{4\left(1-\theta+\frac{\theta h}{2}\right)\left[Y_j + (\frac{\theta h}{2}-1+\theta)Y_j\left(1-Y_j^2\right)\right]Y_0 + \theta^2(1-\frac{h}{2})^2}}{(1-\theta+\frac{\theta h}{2})Y_0}.$$

The relative absolute errors are presented in Tables 5-6.

For the model (2.3), scheme (4.6) becomes

$$\begin{aligned}
H_S^{j+1} &= H_S^j + \left(\frac{1-\theta}{\mathbb{M}(\theta)} + \frac{\theta h}{2\mathbb{M}(\theta)}\right)\left[\pi_H + \gamma_H H_R^{j+1} - \beta_1\varepsilon_1 c H_S^{j+1}V_I^{j+1} - \mu_H H_S^{j+1}\right] \\
&\quad + \left(\frac{\theta h}{2\mathbb{M}(\theta)} - \frac{1-\theta}{\mathbb{M}(\theta)}\right)\left[\pi_H + \gamma_H H_R^j - \beta_1\varepsilon_1 c H_S^j V_I^j - \mu_H H_S^j\right], \\
H_I^{j+1} &= H_I^j + \left(\frac{1-\theta}{\mathbb{M}(\theta)} + \frac{\theta h}{2\mathbb{M}(\theta)}\right)\left[\beta_1\varepsilon_1 c H_S^{j+1}V_I^{j+1} - (\alpha_H + \delta_H + \mu_H)H_I^{j+1}\right] \\
&\quad + \left(\frac{\theta h}{2\mathbb{M}(\theta)} - \frac{1-\theta}{\mathbb{M}(\theta)}\right)\left[\beta_1\varepsilon_1 c H_S^j V_I^j - (\alpha_H + \delta_H + \mu_H)H_I^j\right], \\
H_R^{j+1} &= H_R^j + \left(\frac{1-\theta}{\mathbb{M}(\theta)} + \frac{\theta h}{2\mathbb{M}(\theta)}\right)\left[\alpha_H H_I^{j+1} - (\gamma_H + \mu_H)H_R^{j+1}\right] \\
&\quad + \left(\frac{\theta h}{2\mathbb{M}(\theta)} - \frac{1-\theta}{\mathbb{M}(\theta)}\right)\left[\alpha_H H_I^j - (\gamma_H + \mu_H)H_R^j\right], \\
P^{j+1} &= P^j + \left(\frac{1-\theta}{\mathbb{M}(\theta)} + \frac{\theta h}{2\mathbb{M}(\theta)}\right)\left[\Lambda_P + k\gamma_L L^{j+1}P^{j+1} - (\pi_P + \mu_P)P^{j+1}\right] \\
&\quad + \left(\frac{\theta h}{2\mathbb{M}(\theta)} - \frac{1-\theta}{\mathbb{M}(\theta)}\right)\left[\Lambda_P + k\gamma_L L^j P^j - (\pi_P + \mu_P)P^j\right], \\
L^{j+1} &= L^j + \left(\frac{1-\theta}{\mathbb{M}(\theta)} + \frac{\theta h}{2\mathbb{M}(\theta)}\right)\left[\Lambda_L - (\gamma_L P^{j+1} + \pi_V + \mu_L)L^{j+1}\right] \\
&\quad + \left(\frac{\theta h}{2\mathbb{M}(\theta)} - \frac{1-\theta}{\mathbb{M}(\theta)}\right)\left[\Lambda_L - (\gamma_L P^j + \pi_V + \mu_L)L^j\right], \\
V_S^{j+1} &= V_S^j + \left(\frac{1-\theta}{\mathbb{M}(\theta)} + \frac{\theta h}{2\mathbb{M}(\theta)}\right)\left[\pi_V L^{j+1} - \beta_2\varepsilon_2 c V_S^{j+1}H_I^{j+1} - \mu_V V_S^{j+1}\right] \\
&\quad + \left(\frac{\theta h}{2\mathbb{M}(\theta)} - \frac{1-\theta}{\mathbb{M}(\theta)}\right)\left[\pi_V L^j - \beta_2\varepsilon_2 c V_S^j H_I^j - \mu_V V_S^j\right], \\
V_I^{j+1} &= V_I^j + \left(\frac{1-\theta}{\mathbb{M}(\theta)} + \frac{\theta h}{2\mathbb{M}(\theta)}\right)\left[\beta_2\varepsilon_2 c V_S^{j+1}H_I^{j+1} - \mu_V V_I^{j+1}\right] + \left(\frac{\theta h}{2\mathbb{M}(\theta)} - \frac{1-\theta}{\mathbb{M}(\theta)}\right)\left[\beta_2\varepsilon_2 c V_S^j H_I^j - \mu_V V_I^j\right].
\end{aligned}$$

Simplifying, we have

$$H_S^{j+1} = \frac{H_S^j + \left(\frac{1-\theta}{\mathbb{M}(\theta)} + \frac{\theta h}{2\mathbb{M}(\theta)}\right)\left[\pi_H + \gamma_H H_R^{j+1}\right] + \left(\frac{\theta h}{2\mathbb{M}(\theta)} - \frac{1-\theta}{\mathbb{M}(\theta)}\right)\left[\pi_H + \gamma_H H_R^j - \beta_1\varepsilon_1 c H_S^j V_I^j - \mu_H H_S^j\right]}{1 + \left(\frac{1-\theta}{\mathbb{M}(\theta)} + \frac{\theta h}{2\mathbb{M}(\theta)}\right)\left(\mu_H + \beta_1\varepsilon_1 c V_I^{j+1}\right)}, \quad (6.5)$$

$$H_I^{j+1} = \frac{H_I^j + \left(\frac{1-\theta}{\mathbb{M}(\theta)} + \frac{\theta h}{2\mathbb{M}(\theta)}\right)\beta_1\varepsilon_1 c H_S^{j+1}V_I^{j+1} + \left(\frac{\theta h}{2\mathbb{M}(\theta)} - \frac{1-\theta}{\mathbb{M}(\theta)}\right)\left[\beta_1\varepsilon_1 c H_S^j V_I^j - (\alpha_H + \delta_H + \mu_H)H_I^j\right]}{1 + \left(\frac{1-\theta}{\mathbb{M}(\theta)} + \frac{\theta h}{2\mathbb{M}(\theta)}\right)(\alpha_H + \delta_H + \mu_H)}, \quad (6.6)$$

TABLE 5. Error estimates when $\theta = 0.5$

t	$h = 0.1$		$h = 0.05$		$h = 0.01$	
	PS	ABS	PS	ABS	PS	ABS
0	0	0	0	0	0	0
0.4	2.769×10^{-3}	3.857×10^{-3}	1.332×10^{-3}	1.925×10^{-3}	2.556×10^{-4}	3.812×10^{-4}
0.8	1.666×10^{-3}	3.252×10^{-3}	7.882×10^{-4}	1.607×10^{-3}	1.505×10^{-4}	3.183×10^{-4}
1.2	8.784×10^{-4}	2.491×10^{-3}	4.095×10^{-4}	1.233×10^{-3}	7.722×10^{-5}	2.444×10^{-4}
1.6	3.385×10^{-4}	1.773×10^{-3}	1.500×10^{-4}	8.794×10^{-4}	2.701×10^{-5}	1.746×10^{-4}
2.0	2.396×10^{-5}	1.162×10^{-3}	2.393×10^{-5}	5.776×10^{-4}	6.609×10^{-6}	1.149×10^{-4}

TABLE 6. Error estimates when θ= 0.2

t	$h = 0.1$		$h = 0.05$		$h = 0.01$	
	PS	ABS	PS	ABS	PS	ABS
0	0	0	0	0	0	0
0.4	1.685×10^{-3}	1.919×10^{-3}	8.600×10^{-4}	9.942×10^{-4}	1.702×10^{-4}	1.990×10^{-4}
0.8	1.449×10^{-3}	1.898×10^{-3}	7.146×10^{-4}	9.509×10^{-4}	1.412×10^{-4}	1.901×10^{-4}
1.2	1.200×10^{-3}	1.789×10^{-3}	5.910×10^{-4}	8.945×10^{-4}	1.167×10^{-4}	1.788×10^{-4}
1.6	9.881×10^{-4}	1.664×10^{-3}	4.859×10^{-4}	8.316×10^{-4}	9.589×10^{-5}	1.663×10^{-4}
2.0	8.072×10^{-4}	1.531×10^{-3}	3.964×10^{-4}	7.657×10^{-4}	7.815×10^{-5}	1.531×10^{-4}

$$H_R^{j+1}=\frac{H_R^j+\left(\frac{1-\theta}{M(\theta)}+\frac{\theta h}{2M(\theta)}\right)\alpha_H H_I^{j+1}+\left(\frac{\theta h}{2M(\theta)}-\frac{1-\theta}{M(\theta)}\right)\left[\alpha_H H_I^j-(\gamma_H+\mu_H)H_R^j\right]}{1+\left(\frac{1-\theta}{M(\theta)}+\frac{\theta h}{2M(\theta)}\right)(\gamma_H+\mu_H)}, \quad (6.7$$

$$P^{j+1}=\frac{P^j+\left(\frac{1-\theta}{M(\theta)}+\frac{\theta h}{2M(\theta)}\right)\Lambda_P+\left(\frac{\theta h}{2M(\theta)}-\frac{1-\theta}{M(\theta)}\right)\left[\Lambda_P+k\gamma_L L^j P^j-(\pi_P+\mu_P)P^j\right]}{1+\left(\frac{1-\theta}{M(\theta)}+\frac{\theta h}{2M(\theta)}\right)(\pi_P+\mu_P-k\gamma_L L^{j+1})}, \quad (6.8)$$

$$L^{j+1}=\frac{L^j+\left(\frac{1-\theta}{M(\theta)}+\frac{\theta h}{2M(\theta)}\right)\Lambda_L+\left(\frac{\theta h}{2M(\theta)}-\frac{1-\theta}{M(\theta)}\right)\left[\Lambda_L-(\gamma_L P^j+\pi_V+\mu_L)L^j\right]}{1+\left(\frac{1-\theta}{M(\theta)}+\frac{\theta h}{2M(\theta)}\right)(\gamma_L P^{j+1}+\pi_V+\mu_L)}, \quad (6.9)$$

$$V_S^{j+1}=\frac{V_S^j+\left(\frac{1-\theta}{M(\theta)}+\frac{\theta h}{2M(\theta)}\right)\pi_V L^{j+1}+\left(\frac{\theta h}{2M(\theta)}-\frac{1-\theta}{M(\theta)}\right)\left[\pi_V L^j-\beta_2\varepsilon_2 c V_S^j H_I^j-\mu_V V_S^j\right]}{1+\left(\frac{1-\theta}{M(\theta)}+\frac{\theta h}{2M(\theta)}\right)\left[\beta_2\varepsilon_2 c H_I^{j+1}+\mu_V\right]}, \quad (6.10)$$

$$V_I^{j+1}=\frac{V_I^j+\left(\frac{1-\theta}{M(\theta)}+\frac{\theta h}{2M(\theta)}\right)\beta_2\varepsilon_2 c V_S^{j+1}H_I^{j+1}+\left(\frac{\theta h}{2M(\theta)}-\frac{1-\theta}{M(\theta)}\right)\left[\beta_2\varepsilon_2 c V_S^j H_I^j-\mu_V V_I^j\right]}{1+\left(\frac{1-\theta}{M(\theta)}+\frac{\theta h}{2M(\theta)}\right)\mu_V}, \quad (6.11)$$

Scheme (6.5)-(6.11) is an implicit scheme and therefore difficult to implement. We thus linearize the scheme and obtain

$$H_S^{j+1}=\frac{H_S^j+\left(\frac{1-\theta}{M(\theta)}+\frac{\theta h}{2M(\theta)}\right)\left[\pi_H+\gamma_H\left(2H_R^j-H_R^{j-1}\right)\right]+\left(\frac{\theta h}{2M(\theta)}-\frac{1-\theta}{M(\theta)}\right)\left[\pi_H+\gamma_H H_R^j-\beta_1\varepsilon_1 c H_S^j V_I^j-\mu_H H_S^j\right]}{1+\left(\frac{1-\theta}{M(\theta)}+\frac{\theta h}{2M(\theta)}\right)\left(\mu_H+\beta_1\varepsilon_1 c\left(2V_I^j-V_I^{j-1}\right)\right)}, \quad (6.12)$$

$$H_I^{j+1}=\frac{H_I^j+\left(\frac{1-\theta}{M(\theta)}+\frac{\theta h}{2M(\theta)}\right)\beta_1\varepsilon_1 c\left(2H_S^j-H_S^{j-1}\right)\left(2V_I^j-V_I^{j-1}\right)+\left(\frac{\theta h}{2M(\theta)}-\frac{1-\theta}{M(\theta)}\right)\left[\beta_1\varepsilon_1 c H_S^j V_I^j-(\alpha_H+\delta_H+\mu_H)H_I^j\right]}{1+\left(\frac{1-\theta}{M(\theta)}+\frac{\theta h}{2M(\theta)}\right)(\alpha_H+\delta_H+\mu_H)}, \quad (6.13)$$

$$H_R^{j+1}=\frac{H_R^j+\left(\frac{1-\theta}{M(\theta)}+\frac{\theta h}{2M(\theta)}\right)\alpha_H\left(2H_I^j-H_I^{j-1}\right)+\left(\frac{\theta h}{2M(\theta)}-\frac{1-\theta}{M(\theta)}\right)\left[\alpha_H H_I^j-(\gamma_H+\mu_H)H_R^j\right]}{1+\left(\frac{1-\theta}{M(\theta)}+\frac{\theta h}{2M(\theta)}\right)(\gamma_H+\mu_H)}, \quad (6.14)$$

$$P^{j+1}=\frac{P^j+\left(\frac{1-\theta}{M(\theta)}+\frac{\theta h}{2M(\theta)}\right)\Lambda_P+\left(\frac{\theta h}{2M(\theta)}-\frac{1-\theta}{M(\theta)}\right)\left[\Lambda_P+k\gamma_L L^j P^j-(\pi_P+\mu_P)P^j\right]}{1+\left(\frac{1-\theta}{M(\theta)}+\frac{\theta h}{2M(\theta)}\right)\left(\pi_P+\mu_P-k\gamma_L\left(2L^j-L^{j-1}\right)\right)}, \quad (6.15)$$

$$L^{j+1}=\frac{L^j+\left(\frac{1-\theta}{M(\theta)}+\frac{\theta h}{2M(\theta)}\right)\Lambda_L+\left(\frac{\theta h}{2M(\theta)}-\frac{1-\theta}{M(\theta)}\right)\left[\Lambda_L-(\gamma_L P^j+\pi_V+\mu_L)L^j\right]}{1+\left(\frac{1-\theta}{M(\theta)}+\frac{\theta h}{2M(\theta)}\right)\left(\gamma_L\left(2P^j-P^{j-1}\right)+\pi_V+\mu_L\right)}, \quad (6.16)$$

$$V_S^{j+1}=\frac{V_S^j+\left(\frac{1-\theta}{M(\theta)}+\frac{\theta h}{2M(\theta)}\right)\pi_V\left(2L^j-L^{j-1}\right)+\left(\frac{\theta h}{2M(\theta)}-\frac{1-\theta}{M(\theta)}\right)\left[\pi_V L^j-\beta_2\varepsilon_2 c V_S^j H_I^j-\mu_V V_S^j\right]}{1+\left(\frac{1-\theta}{M(\theta)}+\frac{\theta h}{2M(\theta)}\right)\left[\beta_2\varepsilon_2 c\left(2H_I^j-H_I^{j-1}\right)+\mu_V\right]}, \quad (6.17)$$

$$V_I^{j+1}=\frac{V_I^j+\left(\frac{1-\theta}{M(\theta)}+\frac{\theta h}{2M(\theta)}\right)\beta_2\varepsilon_2 c\left(2V_S^j-V_S^{j-1}\right)\left(2H_I^j-H_I^{j-1}\right)+\left(\frac{\theta h}{2M(\theta)}-\frac{1-\theta}{M(\theta)}\right)\left[\beta_2\varepsilon_2 c V_S^j H_I^j-\mu_V V_I^j\right]}{1+\left(\frac{1-\theta}{M(\theta)}+\frac{\theta h}{2M(\theta)}\right)\mu_V}, \quad (6.18)$$

where $j = 1,2,....$ Scheme (6.12)–(6.18) is not self starting, we therefore obtain the first iterative values using

$$H_S^1=\frac{H_S^0+\left(\frac{1-\theta}{M(\theta)}+\frac{\theta h}{2M(\theta)}\right)\left[\pi_H+\gamma_H H_R^0\right]+\left(\frac{\theta h}{2M(\theta)}-\frac{1-\theta}{M(\theta)}\right)\left[\pi_H+\gamma_H H_R^0-\beta_1\varepsilon_1 c H_S^0 V_I^0-\mu_H H_S^0\right]}{1+\left(\frac{1-\theta}{M(\theta)}+\frac{\theta h}{2M(\theta)}\right)\left(\mu_H+\beta_1\varepsilon_1 c V_I^0\right)},$$

$$H_I^1=\frac{H_I^0+\left(\frac{1-\theta}{M(\theta)}+\frac{\theta h}{2M(\theta)}\right)\beta_1\varepsilon_1 c H_S^0 V_I^0+\left(\frac{\theta h}{2M(\theta)}-\frac{1-\theta}{M(\theta)}\right)\left[\beta_1\varepsilon_1 c H_S^0 V_I^0-(\alpha_H+\delta_H+\mu_H)H_I^0\right]}{1+\left(\frac{1-\theta}{M(\theta)}+\frac{\theta h}{2M(\theta)}\right)(\alpha_H+\delta_H+\mu_H)},$$

$$H_R^1=\frac{H_R^0+\left(\frac{1-\theta}{M(\theta)}+\frac{\theta h}{2M(\theta)}\right)\alpha_H H_I^0+\left(\frac{\theta h}{2M(\theta)}-\frac{1-\theta}{M(\theta)}\right)\left[\alpha_H H_I^0-(\gamma_H+\mu_H)H_R^0\right]}{1+\left(\frac{1-\theta}{M(\theta)}+\frac{\theta h}{2M(\theta)}\right)(\gamma_H+\mu_H)},$$

$$P^1=\frac{P^0+\left(\frac{1-\theta}{M(\theta)}+\frac{\theta h}{2M(\theta)}\right)\Lambda_P+\left(\frac{\theta h}{2M(\theta)}-\frac{1-\theta}{M(\theta)}\right)\left[\Lambda_P+k\gamma_L L^0 P^0-(\pi_P+\mu_P)P^0\right]}{1+\left(\frac{1-\theta}{M(\theta)}+\frac{\theta h}{2M(\theta)}\right)(\pi_P+\mu_P-k\gamma_L L^0)},$$

$$L^1=\frac{L^0+\left(\frac{1-\theta}{M(\theta)}+\frac{\theta h}{2M(\theta)}\right)\Lambda_L+\left(\frac{\theta h}{2M(\theta)}-\frac{1-\theta}{M(\theta)}\right)\left[\Lambda_L-(\gamma_L P^0+\pi_V+\mu_L)L^0\right]}{1+\left(\frac{1-\theta}{M(\theta)}+\frac{\theta h}{2M(\theta)}\right)(\gamma_L P^0+\pi_V+\mu_L)},$$

$$V_S^1=\frac{V_S^0+\left(\frac{1-\theta}{M(\theta)}+\frac{\theta h}{2M(\theta)}\right)\pi_V L^0+\left(\frac{\theta h}{2M(\theta)}-\frac{1-\theta}{M(\theta)}\right)\left[\pi_V L^0-\beta_2\varepsilon_2 c V_S^0 H_I^0-\mu_V V_S^0\right]}{1+\left(\frac{1-\theta}{M(\theta)}+\frac{\theta h}{2M(\theta)}\right)\left[\beta_2\varepsilon_2 c H_I^0+\mu_V\right]},$$

$$V_I^1=\frac{V_I^0+\left(\frac{1-\theta}{M(\theta)}+\frac{\theta h}{2M(\theta)}\right)\beta_2\varepsilon_2 c V_S^0 H_I^0+\left(\frac{\theta h}{2M(\theta)}-\frac{1-\theta}{M(\theta)}\right)\left[\beta_2\varepsilon_2 c V_S^0 H_I^0-\mu_V V_I^0\right]}{1+\left(\frac{1-\theta}{M(\theta)}+\frac{\theta h}{2M(\theta)}\right)\mu_V}.$$